

# Electrically tuneable nonlinear anomalous Hall effect in two-dimensional transition-metal dichalcogenides $\text{WTe}_2$ and $\text{MoTe}_2$

Yang Zhang,<sup>1,2</sup> Jeroen van den Brink,<sup>2,3</sup> Claudia Felser,<sup>1</sup> and Binghai Yan<sup>4,\*</sup>

<sup>1</sup>Max Planck Institute for Chemical Physics of Solids, 01187 Dresden, Germany

<sup>2</sup>Leibniz Institute for Solid State and Materials Research, IFW Dresden, 01069 Dresden, Germany

<sup>3</sup>Institut für Theoretische Physik, TU Dresden, 01062 Dresden, Germany

<sup>4</sup>Department of Condensed Matter Physics, Weizmann Institute of Science, Rehovot, 7610001, Israel

We studied the nonlinear electric response in  $\text{WTe}_2$  and  $\text{MoTe}_2$  monolayers. When the inversion symmetry is breaking but the the time-reversal symmetry is preserved, a second-order Hall effect called the nonlinear anomalous Hall effect (NLAHE) emerges owing to the nonzero Berry curvature on the nonequilibrium Fermi surface. We reveal a strong NLAHE with a Hall-voltage that is quadratic with respect to the longitudinal current. The optimal current direction is normal to the mirror plane in these two-dimensional (2D) materials. The NLAHE can be sensitively tuned by an out-of-plane electric field, which induces a transition from a topological insulator to a normal insulator. Crossing the critical transition point, the magnitude of the NLAHE increases, and its sign is reversed. Our work paves the way to discover exotic nonlinear phenomena in inversion-symmetry-breaking 2D materials.

## I. INTRODUCTION

The past decade has seen intensive investigation of band-structure topology and the discovery of novel topological states and topological materials, such as topological insulators (TIs)<sup>1-4</sup> and topological Dirac and Weyl semimetals<sup>5-11</sup>. The band-structure topology and electronic response functions are commonly characterised by the Berry curvature<sup>12</sup> in the momentum( $k$ ) space. A well-established example is the anomalous Hall effect<sup>13</sup> as an intrinsic property originating in the band structure, in which the Berry curvature integrated over the occupied states at the thermodynamic equilibrium gives rise to the Hall conductivity. The anomalous Hall effect and its quantised version have recently been observed in time-reversal symmetry (TRS) breaking topological materials, for example, magnetically doped TIs<sup>14-16</sup> and magnetic Weyl semimetals<sup>17-20</sup>. In recent years there has been increasing interest in the nonlinear optical and electrical properties of topological materials, considering the Berry phase effect<sup>21-25</sup>.

In the linear response regime, the anomalous Hall effect vanishes in the presence of TRS, because TRS forces the Berry curvature to be odd with respect to  $k$ , i.e.  $\Omega^n(k) = -\Omega^n(-k)$  where  $n$  is the band index. In the nonlinear response regime, however, an intriguing nonlinear anomalous Hall effect (NLAHE) can still survive in the presence of TRS but the absence of the inversion symmetry<sup>26</sup>. When an electric field  $E$  drives a current through a crystal in the steady state, the system is out of equilibrium and the Fermi surface exhibits an effective shift in  $k$ -space. Therefore, the Fermi occupations at  $k$  and  $-k$  are no longer necessarily the same any more. This leads to a net Berry curvature summed on the nonequilibrium Fermi surface, i.e., an anomalous Hall conductivity that is proportional to  $E$  and the relaxation time  $\tau$ . Thus, the Hall voltage is estimated to be quadratic, rather

than linear, to the longitudinal electric field  $E$ . The NLAHE was derived at the zero-frequency limit of the nonlinear photocurrent generation<sup>26,27</sup>. Although it is a nonequilibrium property, the NLAHE can be described by a geometric quantity at the equilibrium Fermi surface, the Berry curvature dipole (BCD)<sup>26</sup>. Very recently the BCD induced NLAHE was calculated for the three-dimensional (3D) Weyl semimetals based on *ab initio* band structures<sup>28</sup> and also for tellurium<sup>29</sup>.

The transition-metal dichalcogenides  $\text{WTe}_2$  and  $\text{MoTe}_2$  are WSMs in the 3D bulk<sup>30,31</sup> and become two-dimensional (2D) TIs in the monolayer (ML) form<sup>32-35</sup>. Nonlinear optical phenomena, for example, a nonlinear photocurrent, were recently reported in their bulk systems<sup>36,37</sup>. In this work, we investigate the NLAHE in MLs of  $\text{WTe}_2$  and  $\text{MoTe}_2$ , because the use of MLs makes it easier to tune the band structure by an external electric field, for instance, by applying a back gate<sup>35</sup>. The out-of-plane electric field is found to sensitively tune the band structure and consequently control the BCD, which is an intrinsic property determined by the band structure and wave functions. Near the electric-field-induced topological transition from a TI to a normal insulator, the BCD and NLAHE are found to be strongly enhanced.

## II. METHODS

The WSM state of  $\text{WTe}_2$  or  $\text{MoTe}_2$  refers to the  $T_d$  phase of the crystal structure (space group  $Pmn2_1$ , No. 31), in which inversion symmetry is broken. However, the corresponding ML recovers the inversion symmetry by a slight distortion, commonly called the  $1T'$  phase (space group  $P2_1/m$ , No. 11). This inversion symmetry can be broken by applying an out-of-plane electric field ( $E$ ) or even by the existence of a substrate. We focus on the  $1T'$ -MLs of the two compounds under different

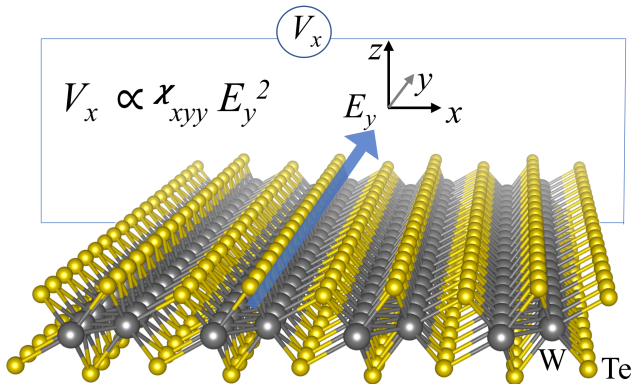


FIG. 1. Crystal structure and the nonlinear anomalous Hall effect in the  $\text{WTe}_2$  monolayer. W and Te atoms are represented by gray and yellow spheres. When applying an electric field along the  $y$  axis, i.e. the W chain direction that crosses the mirror plane, a Hall-like voltage  $V_x$  appears and is quadratic to the electric field  $E_y$ . Such a nonlinear anomalous Hall effect exists without breaking the time-reversal symmetry.

electric fields for two compounds. In addition, we also investigate the  $T_d$ -MLs for comparison, considering the fact that the phase transition may occur under special conditions (e.g. Refs 38 and 39). Both  $T_d$ - and  $1T'$ -MLs share a mirror plane  $\mathcal{M}_y : y \rightarrow -y$ . A zigzag-shape Mo or W atomic chain forms and crosses the mirror plane. The  $\mathcal{M}_y$  symmetry is crucial to determining the symmetry of the NLAHE as we will discuss.

We first perform *ab initio* density-functional theory (DFT) calculations and then project the DFT band structure to atomic-like Wannier functions with FPLO<sup>40</sup>. Starting with the one-particle Hamiltonian ( $\hat{H}$ ) in the basis of Wannier functions, we compute the distribution of the Berry curvature  $\Omega^n(\mathbf{k})$  in the momentum space ( $\mathbf{k}$ ). In a 2D system,  $\Omega^n(\mathbf{k})$  only has a  $z$  component<sup>12</sup>,

$$\Omega_z^n(\mathbf{k}) = 2i\hbar^2 \sum_{m \neq n} \frac{\langle n | \hat{v}_x | m \rangle \langle m | \hat{v}_y | n \rangle}{(\epsilon_n - \epsilon_m)^2}, \quad (1)$$

where  $\epsilon_n$  and  $|n\rangle$  are eigenvalues and eigen wave functions, respectively, of  $\hat{H}$  at the momentum  $\mathbf{k}$  and  $\hat{v}_{x,y} = \frac{d\hat{H}}{\hbar dk_{x,y}}$  the velocity perator.

The nonlinear responses includes the dc current  $j_a^{(0)} = \chi_{abc} \mathcal{E}_b \mathcal{E}_c^*$  and the second harmonic generation  $j_a^{(2\omega)} = \chi_{abc} \mathcal{E}_b \mathcal{E}_c$ , under the oscillating electric field  $E_c(t) = \text{Re}\{\mathcal{E}_c e^{i\omega t}\}$  of light, where  $a, b, c = x, y, z$ . At the zero- $\omega$  limit, the dc current still preserves  $j_a = 2j_a^{(0)}|_{\omega \rightarrow 0} = 2\chi_{abb} |\mathcal{E}_b|^2$ , leading to the so-called NLAHE<sup>26</sup>. Although the NLAHE is related to the net Berry curvature due to a nonequilibrium Fermi distribution, the nonlinear conductivity  $\chi_{abb}$  can be describe by the BCD, a quantity defined in the equilibrium state in the semiclassical

approximation<sup>26</sup> as follows,

$$\chi_{abb} = -\varepsilon_{adb} \frac{e^3 \tau}{2\hbar^2 (1 + i\omega\tau)} D_{bd} \quad (2)$$

$$D_{bd} = \int_{\mathbf{k}} f_n^0(\mathbf{k}) \frac{\partial \Omega_d^n}{\partial k_b}, \quad (3)$$

where  $D_{bd}$  is the BCD,  $f_n^0(\mathbf{k})$  the equilibrium Fermi-Dirac distribution,  $\tau$  the relaxation time,  $\varepsilon_{adb}$  the third rank Levi-Civita symbol,  $a, b = x, y$  and  $d = z$  in 2D. We compute  $\Omega_d$  by Eq. 1 and then calculate the  $D_{bd}$  by integrating  $\frac{\partial \Omega_d^n}{\partial k_b}$  in a very dense  $k$ -grid ( $2000 \times 2000$ ) to obtain converged values of the BCD. The BCD is dimensionless in three dimensions, whereas it is in unit of length in 2D.

Because  $\Omega_z^n$  is odd with respect to the  $\mathcal{M}_y$  reflection,  $\frac{\partial \Omega_z^n}{\partial k_x}$  is odd to  $\mathcal{M}_y$  while only  $\frac{\partial \Omega_z^n}{\partial k_y}$  is even. Therefore, only  $D_{yz}$  and  $\chi_{xyy}$  are nonzero. Thus, the nonlinear Hall voltage  $V_x$  appears inside the mirror plane when an electric field  $E_y$  passes along the W or Mo chains, and  $V_x \propto \chi_{xyy} E_y^2$ , as illustrated in Fig. 1. If the voltage contacts and electric field directions are switched, there will be no NLAHE signal. This a strong anisotropy can serve as a useful tool to distinguish the NLAHE from other effects in  $\text{WTe}_2$  and  $\text{MoTe}_2$  MLs.

### III. RESULTS AND DISCUSSION

#### A. $1T'$ Monolayers of $\text{WTe}_2$

We start with the  $1T'$ -ML of  $\text{WTe}_2$ . It is known to be a 2D TI. An applied electric field breaks the inversion symmetry and induce a transition from a TI to a trivial insulator. During the transition, the band gap first shrinks to zero and then opens again. A previous study on the TaAs-family of WSMs<sup>28</sup> revealed that the small gap or zero gap region contributes a large gradient of the Berry curvature, i.e, a large BCD. This can be intuitively understood from Eq. 1. The smallness of the energy gap (i.e, the denominator of Eq. 1) usually indicates that a large Berry curvature is concentrated on the small gap region, which is usually a narrow momentum area, leading to a large gradient of the Berry curvature. In addition to a large magnitude of the BCD, a sign change of the BCD may be induced by the phase transition, because the band inversion switches the sign of the Berry curvature. Therefore, we are particularly interested in the evolution of the BCD with respect to the topological phase transition.

Figure 2 shows the band structures of the  $1T'$ -ML under various electric fields. At  $E = 0$ , all the bands are doubly degenerate because of the coexistence of TRS and the inversion symmetry. The band structure exhibits direct band gaps with an inversion between the conduction and valence bands, giving rise to the 2D TI phase. The zero indirect band gap is due to the known DFT underestimation, whereas the quasiparticle

energy correction can lift the indirect gap, as discussed in previous work<sup>32</sup>. Because this gap underestimation does not affect the Berry curvature effect investigated here, for simplicity, we use the DFT band structures in this work. As  $E$  increases, we indeed observe that the direct energy gap shrinks to zero at  $E = 0.0075$  V/ $a_0$  ( $a_0$  is the Bohr radius, 0.53 Å) and opens again, inducing the topological transition. We note that the band touching point at the critical electric field is not equivalent to a Weyl point, since it is not stable against a weak perturbation (e.g. the variation of  $E$ ) and the Weyl point is well-defined only for 1D and 3D systems. The  $Z_2$  topological invariant before and after the transition is verified by tracing the Wannier centres by the Wilson loop method<sup>41,42</sup>.

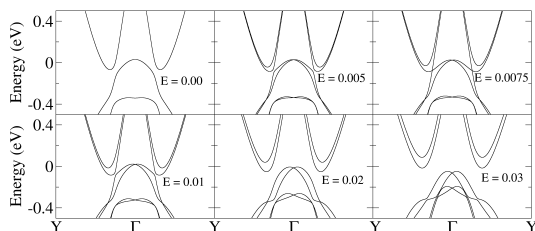


FIG. 2. Band structures of  $\text{WTe}_2$   $1T'$ -monolayers with applied electric field. The electric field  $E$  is out-of-plane and in unit of  $\text{eV}/a_0$ , where  $a_0$  is the Bohr radius. The band dispersion is shown along the  $\Gamma$ -Y direction, i.e. along the zigzag W chain.

We show the corresponding BCD in Figure 3. At  $E = 0$ , the BCD vanishes regardless of position of the Fermi energy ( $E_F$ ), because the coexistence of TRS and inversion symmetry forces  $\Omega(\mathbf{k}) = 0$  at every momentum  $\mathbf{k}$ . At  $E = 0.005$  V/ $a_0$  (the TI phase), a large BCD appears (Fig. 3a). Because it is a Fermi surface property, the BCD depends sensitively on the position of  $E_F$ . We focus on the BCD for  $E_F = 0$ , i.e. the charge neutral point. As  $E$  increases from zero, the BCD varies nonmonotonically and is characterised by four regimes. It (i) first increases in a positive amplitude (e.g.  $E = 0.005$ ), (ii) then reduces to zero (near  $E = 0.0075$ ), (iii) further grows with a negative amplitude (e.g.  $E = 0.01$ ), and (iv) finally decreases to zero at large  $E$  ( $E > 0.03$ ). The regime-(i) is caused by the emergence of nonzero BCD by breaking the inversion symmetry with  $E$ . Because the phase transition switches the order of the conduction and valence bands, the sign of the Berry curvature is reversed by the transition, and thus the sign of the BCD is also reversed for regimes-(ii) and (iii). This behaviour is quite similar to the sign change of the photocurrent calculated at the topological phase transition of TIs<sup>43</sup>. At large  $E$ , the system becomes a gapped insulator; thus, the Fermi surface vanishes at  $E_F = 0$  and the BCS then becomes zero. This behaviour explains the regime-(iv). For  $E = 0.005$  and 0.01, one

can find a peak of BCD slightly below  $E_F = 0$  in Fig. 3. This is because the smallest energy-gap (the largest Berry curvature) appears slightly below  $E_F = 0$ .

When the BCD is projected to 2D  $k$ -space, it is easier to understand the BCD from the corresponding band structure. For example, at  $E = 0.005$  the BCD is predominantly contributed by the small-gap region, for example, the nearly band touching positions along the  $\Gamma$ -Y line. After the band inversion at  $E = 0.01$ , the BCD indeed changes sign. As  $E$  increases further to  $E = 0.02$  and  $E = 0.03$ , the BCD decreases exponentially in amplitude, corresponding to regime-(iv) discussed above.

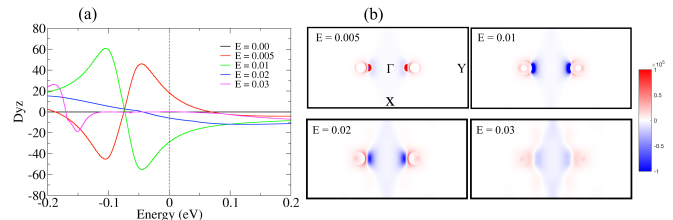


FIG. 3. The Berry curvature dipole at different Fermi energy and its distribution in the 2D Brillouin zone for  $\text{WTe}_2$   $1T'$ -monolayers with varying applied electric field. The Berry curvature dipole is in unit of  $a_0$ , where  $a_0$  is the Bohr radius 0.529 Å. In the 2D Brillouin zone, red and blue colors present positive and negative amplitudes (in arbitrary units) of the Berry curvature dipole.

## B. $T_d$ Monolayers of $\text{WTe}_2$

The  $T_d$ -ML breaks inversion symmetry. We can divide the effect of inversion symmetry breaking into two parts, the in-plane distortion  $\Delta_{\parallel}$  and the out-of-plane distortion  $\Delta_{\perp}$ . The induced band splitting can be observed at the bottom of the conduction band (Fig. 4a). It is also a 2D TI in topology. When an electric field is applied along the  $\Delta_{\perp}$ , the symmetry breaking can be further enhanced to be  $\Delta_{\parallel} + E$ . For example, both the conduction and valence bands split further as  $E$  increases from 0 to 0.05. As in the  $1T'$  structure,  $E$  drives the system to the topological phase transition in the band structure. However, the critical field for the  $T_d$  phase ( $\sim 0.10$ ) is much larger than that for the  $1T'$  phase. Therefore, the BCD increases monotonically from  $E = 0$  to  $E = 0.05$ , as shown in Fig. 4b. When  $E$  is opposite to  $\Delta_{\perp}$ , the effective out-of-plane inversion-symmetry-breaking is  $\Delta_{\perp} - E$ . As  $E$  increases in amplitude, the symmetry-breaking effect first decreases and then increase again. For example, the band splitting is partially suppressed for  $E = -0.01$  and is further enhanced for  $E = -0.05$ . The BCD shows the same trend (see Fig. 4b).

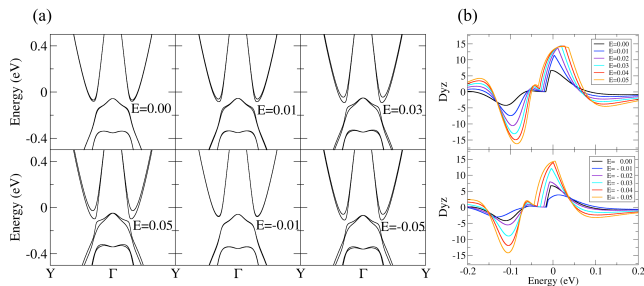


FIG. 4. Band structures and the Berry curvature dipole (in unit of  $a_0$ ) at different electric field ( $E$  in unit of  $V/a_0$ ) for  $WTe_2$   $T_d$ -monolayers.

### C. Monolayers of $MoTe_2$

The  $MoTe_2$  MLs ( $1T'$  and  $T_d$ ) exhibit trends quite similar to those of  $WTe_2$  MLs. For the  $1T'$  structure, the topological phase transition occurs between  $E = 0.01$  and  $E = 0.015$ . Therefore, the BCD exhibits large magnitudes with opposite signs under these two electric fields. When  $E$  increases further, the BCD decreases in amplitude, as shown in Fig. 5.

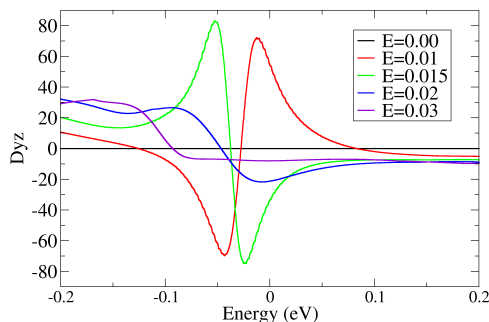


FIG. 5. The Berry curvature dipole at different Fermi energy for  $MoTe_2$   $1T'$ -monolayers with varying applied electric field.

### D. Discussions

We estimate the magnitude of the NLAHE. In a longitudinal dc field  $E_y$ , the nonlinear Hall  $j_x =$

$2j_x^{(0)}|_{\omega \rightarrow 0} = 2\chi_{xyy}|\mathcal{E}_y|^2 = \sigma_{xy}E_y$ , where we define a Hall conductance  $\sigma_{xy} \equiv 2\chi_{xyy}E_y = \frac{e^3\tau}{\hbar^2}D_{yz} = G_0(\tau D_{yz}eE_y\pi/\hbar)$  and  $G_0 \equiv \frac{2e^2}{h}$  the conductance quantum. Considering  $E_y \sim 10^3$  V/m,  $\tau \sim 1$  ps and  $D_{yz} \sim 20a_0$  for  $1T'$   $WTe_2$ , we obtain  $\sigma_{xy} \sim 1\%G_0$ . The magnitude of the NLAHE in  $MoTe_2$ -MLs is comparable to that of  $WTe_2$ , as indicated in Fig. 5. This Hall conductance can be measured under current experimental conditions.

## IV. CONCLUSIONS

In conclusion, we reveal a strong NLAHE in  $WTe_2$  and  $MoTe_2$  MLs. An out-of-plane external electric field can break the inversion symmetry (for the  $1T'$  structure) and generate a nonzero BCD, leading to the NLAHE. Near the topological phase transition region induced by the electric field, the NLAHE is strongly enhanced. In addition to a dc electric field, a longitudinal (in-plane) electric field can also be the electric field of a low-frequency stimulation (e.g. a microwave), which may induce an even stronger NLAHE owing to the strong electric field. In addition to an out-of-plane electric field, the inversion symmetry of MLs can also be broken by other ways, such as the strain (e.g. recently realised in the  $MoS_2$  ML<sup>44</sup>) and the substrate proximity. Note that our conclusions can be generalised from MLs to few layers and also to other phases (e.g.  $2H$  and  $1T$ ) of transition-metal dichalcogenides, when the inversion symmetry as well as the three-fold rotational symmetry is broken in these systems.

## V. ACKNOWLEDGMENTS

Y.Z., J.vdB. and C.F. thank financial support by the German Research Foundation (DFG, SFB 1143). C.F. acknowledges the European Research Council (ERC) Advanced Grant (No. 742068) ‘‘TOPMAT’’. B.Y. is supported by a research grant from the Benozziyo Endowment Fund for the Advancement of Science.

\* binghai.yan@weizmann.ac.il

<sup>1</sup> X.-L. Qi and S.-C. Zhang, Rev. Mod. Phys. **83**, 1057 (2011).

<sup>2</sup> M. Z. Hasan and C. L. Kane, Rev. Mod. Phys. **82**, 3045 (2010).

<sup>3</sup> B. Yan and S.-C. Zhang, Rep. Prog. Phys. **75**, 096501 (2012).

- <sup>4</sup> Y. Ando, *J. Phys. Soc. Jp.* **82**, 102001 (2013).
- <sup>5</sup> X. G. Wan, A. M. Turner, A. Vishwanath, and S. Y. Savrasov, *Phys. Rev. B* **83**, 205101 (2011).
- <sup>6</sup> G. E. Volovik, *The Universe in A Helium Droplet* (Clarendon Press, Oxford, 2003).
- <sup>7</sup> S. Murakami, *New J. Phys.* **9**, 356 (2007).
- <sup>8</sup> A. A. Burkov, M. D. Hook, and L. Balents, *Phys. Rev. B* **84**, 235126 (2011).
- <sup>9</sup> P. Hosur and X. L. Qi, *C. R. Physique* **14**, 857 (2013).
- <sup>10</sup> B. Yan and C. Felser, *Annual Review of Condensed Matter Physics* **8**, 337 (2017).
- <sup>11</sup> N. P. Armitage, E. J. Mele, and A. Vishwanath, *Rev. Mod. Phys.* **90**, 015001 (2018).
- <sup>12</sup> D. Xiao, M.-C. Chang, and Q. Niu, *Rev. Mod. Phys.* **82**, 1959 (2010).
- <sup>13</sup> N. Nagaosa, J. Sinova, S. Onoda, A. H. MacDonald, and N. P. Ong, *Reviews of Modern Physics* **82**, 1539 (2010).
- <sup>14</sup> C.-X. Liu, X.-L. Qi, X. Dai, Z. Fang, and S.-C. Zhang, *Phys. Rev. Lett.* **101** (2008).
- <sup>15</sup> R. Yu, W. Zhang, H. J. Zhang, S. C. Zhang, X. Dai, and Z. Fang, *Science* **329**, 61 (2010).
- <sup>16</sup> C. Chang, J. Zhang, X. Feng, J. Shen, Z. Zhang, M. Guo, K. Li, Y. Ou, P. Wei, L. Wang, Z. Q. Ji, Y. Feng, S. Ji, X. Chen, J. Jia, X. Dai, Z. Fang, S. C. Zhang, K. He, Y. Wang, L. Lu, X. C. Ma, and Q.-K. Xue, *Science* **340**, 167 (2013).
- <sup>17</sup> G. Xu, H. Weng, Z. Wang, X. Dai, and Z. Fang, *Phys. Rev. Lett.* **107**, 186806 (2011).
- <sup>18</sup> K.-Y. Yang, Y.-M. Lu, and Y. Ran, *Phys. Rev. B* **84**, 075129 (2011).
- <sup>19</sup> A. A. Burkov, *Phys. Rev. Lett.* **113** (2014).
- <sup>20</sup> H. Yang, Y. Sun, Y. Zhang, W.-J. Shi, S. S. P. Parkin, and B. Yan, *N. J. Phys.* **19**, 015008 (2017).
- <sup>21</sup> J. E. Moore and J. Orenstein, *Phys. Rev. Lett.* **105**, 026805 (2010).
- <sup>22</sup> E. Deyo, L. E. Golub, E. L. Ivchenko, and B. Spivak, *arxiv* (2009), 0904.1917.
- <sup>23</sup> S. M. Young and A. M. Rappe, *Phys. Rev. Lett.* **109**, 116601 (2012).
- <sup>24</sup> J. E. Sipe and A. I. Shkrebtii, *Phys. Rev. B* **61**, 5337 (2000).
- <sup>25</sup> T. Morimoto and N. Nagaosa, *Science Advances* **2**, e1501524 (2016).
- <sup>26</sup> I. Sodemann and L. Fu, *Phys. Rev. Lett.* **115**, 216806 (2015).
- <sup>27</sup> T. Morimoto, S. Zhong, J. Orenstein, and J. E. Moore, *Phys. Rev. B* **94**, 245121 (2016).
- <sup>28</sup> Y. Zhang, Y. Sun, and B. Yan, *Phys. Rev. B* **97**, 041101 (R) (2018).
- <sup>29</sup> S. S. Tsirkin, P. A. Puente, and I. Souza, *Phys. Rev. B* **97**, 035158 (2018).
- <sup>30</sup> A. A. Soluyanov, D. Gresch, Z. Wang, Q. Wu, M. Troyer, X. Dai, and B. A. Bernevig, *Nature* **527**, 495 (2015).
- <sup>31</sup> Y. Sun, S. C. Wu, M. N. Ali, C. Felser, and B. Yan, *Phys. Rev. B* **92**, 161107(R) (2015).
- <sup>32</sup> X. Qian, J. Liu, L. Fu, and J. Li, *Science* **346**, 1344 (2014).
- <sup>33</sup> S. Tang, C. Zhang, D. Wong, Z. Pedramrazi, H.-Z. Tsai, C. Jia, B. Moritz, M. Claassen, H. Ryu, S. Kahn, J. Jiang, H. Yan, M. Hashimoto, D. Lu, R. G. Moore, C.-C. Hwang, C. Hwang, Z. Hussain, Y. Chen, M. M. Ugeda, Z. Liu, X. Xie, T. P. Devereaux, M. F. Crommie, S.-K. Mo, and Z.-X. Shen, *Nature Physics* **13**, 683 (2017).
- <sup>34</sup> L. Peng, Y. Yuan, G. Li, X. Yang, J.-J. Xian, C.-J. Yi, Y.-G. Shi, and Y.-S. Fu, *Nat. Commun.* **8**, 659 (2017).
- <sup>35</sup> S. Wu, V. Fatemi, Q. D. Gibson, K. Watanabe, T. Taniguchi, R. J. Cava, and P. Jarillo-Herrero, *Science* **359**, 76 (2018).
- <sup>36</sup> S. Lim, C. R. Rajamathi, V. Suß, C. Felser, and A. Kapitulnik, *arXiv* (2018), 1802.02838.
- <sup>37</sup> Z. Ji, G. Liu, Z. Addison, W. Liu, P. Yu, H. Gao, Z. Liu, A. M. Rappe, C. L. Kane, E. J. Mele, and R. Agarwal, (2018), 1802.04387.
- <sup>38</sup> Y. Qi, P. G. Naumov, M. N. Ali, C. R. Rajamathi, W. Schnelle, O. Barkalov, M. Hanfland, S.-C. Wu, C. Shekhar, Y. Sun, V. Suß, M. Schmidt, U. Schwarz, E. Pippel, P. Werner, R. Hillebrand, T. Forster, E. Kampert, S. Parkin, R. J. Cava, C. Felser, B. Yan, and S. A. Medvedev, *Nat. Commun.* **7**, 11038 (2016).
- <sup>39</sup> J. Yang, J. Colen, J. Liu, M. C. Nguyen, G.-w. Chern, and D. Louca, *Science advances* **3**, eaao4949 (2017).
- <sup>40</sup> K. Koepf and H. Eschrig, *Phys. Rev. B* **59**, 1743 (1999), [www.fpl.de](http://www.fpl.de).
- <sup>41</sup> R. Yu, X. L. Qi, A. Bernevig, Z. Fang, and X. Dai, *Phys. Rev. B* **84** (2011).
- <sup>42</sup> A. A. Soluyanov and D. Vanderbilt, *Phys. Rev. B* **83** (2011).
- <sup>43</sup> L. Z. Tan and A. M. Rappe, *Phys. Rev. Lett.* **116**, 237402 (2016).
- <sup>44</sup> J. Lee, Z. Wang, H. Xie, K. F. Mak, and J. Shan, *Nature Materials* **16**, 887 (2017).